

RESEARCH ARTICLE | DECEMBER 03 2024

## Novel pseudo-hexagonal montmorillonite model and microsecond MD simulations of hydrate formation in mixed clay sediments with surface defects

Special Collection: [Molecular Dynamics, Methods and Applications 60 Years after Rahman](#)

Fengyi Mi  ; Jiangtao Pang  ; Wei Li  ; Othonas A. Moullos  ; Fulong Ning  ; Thijs J. H. Vlugt 



*J. Chem. Phys.* 161, 214703 (2024)

<https://doi.org/10.1063/5.0235454>



View  
Online



Export  
Citation

### Articles You May Be Interested In

Transforming underground to surface mining operation – A geotechnical perspective from case study

*AIP Conference Proceedings* (November 2021)

Monthly prediction of rainfall in nickel mine area with artificial neural network

*AIP Conference Proceedings* (November 2021)

Estimation of Karts groundwater based on geophysical methods in the Monggol Village, Saptosari District, Gunungkidul Regency

*AIP Conference Proceedings* (November 2021)

# Novel pseudo-hexagonal montmorillonite model and microsecond MD simulations of hydrate formation in mixed clay sediments with surface defects

Cite as: J. Chem. Phys. 161, 214703 (2024); doi: 10.1063/5.0235454

Submitted: 27 August 2024 • Accepted: 14 November 2024 •

Published Online: 3 December 2024



View Online



Export Citation



CrossMark

Fengyi Mi,<sup>1,2</sup> Jiangtao Pang,<sup>1</sup> Wei Li,<sup>1</sup> Othonas A. Moultos,<sup>2</sup> Fulong Ning,<sup>1,a)</sup> and Thijs J. H. Vlugt<sup>2,a)</sup>

## AFFILIATIONS

<sup>1</sup> National Center for International Research on Deep Earth Drilling and Resource Development, Faculty of Engineering, China University of Geosciences, Wuhan, Hubei 430074, China

<sup>2</sup> Engineering Thermodynamics, Process and Energy Department, Faculty of Mechanical Engineering, Delft University of Technology, Leeghwaterstraat 39, Delft 2628CB, The Netherlands

**Note:** This paper is part of the JCP Special Topic on Molecular Dynamics, Methods and Applications 60 Years After Rahman.

**a)** Authors to whom correspondence should be addressed: [nflzx@cug.edu.cn](mailto:nflzx@cug.edu.cn) and [t.j.h.vlugt@tudelft.nl](mailto:t.j.h.vlugt@tudelft.nl)

## ABSTRACT

Both CH<sub>4</sub> hydrate accumulation and hydrate-based CO<sub>2</sub> sequestration involve hydrate formation in mixed clay sediments. The development of realistic clay models and a nanoscale understanding of hydrate formation in mixed clay sediments are crucial for energy recovery and carbon sequestration. Here, we propose a novel molecular model of pseudo-hexagonal montmorillonite nanoparticles. The stress-strain curves of tension, compression, and shear of pseudo-hexagonal montmorillonite nanoparticles exhibit linear characteristics, with tension, compression, and shear moduli of ~435, 410, and 137 GPa, respectively. We perform microsecond molecular dynamics simulations to study CH<sub>4</sub> and CH<sub>4</sub>/CO<sub>2</sub> hydrate formation in montmorillonite-illite mixed clay sediments with surface defects. The results indicate that hydrate formation in mixed clay sediments is significantly influenced by the presence of clay defects. CH<sub>4</sub> and CH<sub>4</sub>/CO<sub>2</sub> mixed hydrates are challenging to form at the junction between the inside and outside clay defects. CH<sub>4</sub> and CH<sub>4</sub>/CO<sub>2</sub> mixed hydrates exhibit a preference for forming outside the clay defects rather than inside the clay defects. Some CH<sub>4</sub> and CO<sub>2</sub> molecules from the inside clay defect migrate to the outside clay defect, thereby promoting CH<sub>4</sub> and CH<sub>4</sub>/CO<sub>2</sub> mixed hydrate formation outside the clay defects. This molecular insight advances the development of clay particle models and expands an understanding of natural gas hydrate accumulation and hydrate-based CO<sub>2</sub> sequestration.

© 2024 Author(s). All article content, except where otherwise noted, is licensed under a Creative Commons Attribution (CC BY) license (<https://creativecommons.org/licenses/by/4.0/>). <https://doi.org/10.1063/5.0235454>

## I. INTRODUCTION

The increasing demand for traditional fossil energy has spurred the quest for sustainable alternative energy sources.<sup>1</sup> Natural gas hydrates, primarily composed of methane (CH<sub>4</sub>) and water, are crystalline compounds in which CH<sub>4</sub> molecules are encapsulated within a cage-like network of water molecules.<sup>2–5</sup> The estimated reserves of CH<sub>4</sub> hydrates are  $\sim 3 \times 10^{15}$  m<sup>3</sup>, representing the largest source of hydrocarbons globally, with a carbon content roughly twice that of traditional fossil fuels.<sup>6,7</sup> Evidence suggests that extracting CH<sub>4</sub>

energy from natural CH<sub>4</sub> hydrates is feasible from oceanic sediments, with over 90% of CH<sub>4</sub> hydrates located in shallow oceanic sediments.<sup>8,9</sup> The exploitation of CH<sub>4</sub> hydrates in oceanic sediments is a critical step toward transitioning to a low-carbon energy structure. In addition, the injection of CO<sub>2</sub> into seafloor reservoirs to form CO<sub>2</sub> hydrates, i.e., hydrate-based CO<sub>2</sub> sequestration, offers a promising approach for long-term stability, high-capacity CO<sub>2</sub> sequestration.<sup>10,11</sup> The CH<sub>4</sub>-CO<sub>2</sub> replacement method is also considered for its potential to simultaneously facilitate energy recovery, carbon sequestration, and reservoir stabilization.<sup>12</sup> Challenges such

as low gas production efficiency, mass transfer limitations, and environmental risks hinder the commercialization of CH<sub>4</sub> hydrate exploitation and hydrate-based CO<sub>2</sub> sequestration.<sup>13–15</sup> The root of these problems has been traced to the formation of CH<sub>4</sub>/CO<sub>2</sub> hydrates in oceanic sediments. A deep understanding of the formation mechanisms of gas hydrates in seafloor sediments is essential for advancing CH<sub>4</sub> hydrate exploitation and hydrate-based CO<sub>2</sub> sequestration.

More than 90% of the global natural gas hydrates are buried in clay-rich, fine-grained marine sediments, with clay content reaching up to 30% in hydrate-bearing sediments in the Shenhua area of the South China Sea.<sup>8</sup> These high clay contents primarily consist of montmorillonite, illite, and montmorillonite–illite mixed clays. Clay minerals possess unique characteristics such as a fine particle size (<4 μm), a negative surface charge, a high specific area, and strong interfacial reactivity, of which all inevitably influence the formation of gas hydrates in clay-rich oceanic sediments.<sup>16,17</sup> Clay particles promote hydrate formation by providing high water dispersibility, large gas–liquid contact area, and more nucleation sites.<sup>18–21</sup> Fine-grained clay creates a large number of nanoscale confined spaces, which decrease the activity of water molecules and hinder the mass transfer of gas molecules, thus being unfavorable for the formation of gas hydrates.<sup>22–24</sup> Recent experimental investigations have found that the presence of swelling montmorillonite clay promotes the nucleation while slowing the growth kinetics of CH<sub>4</sub> hydrates.<sup>25,26</sup> The unique characteristics of clay and the complexity of the sedimentary environment significantly influence gas hydrate formation, thereby complicating the overall hydrate formation process. Experimental methods alone are insufficient to elucidate these microscopic processes, necessitating the use of advanced techniques. Molecular dynamics (MD) simulation is an emerging tool for revealing and studying the formation mechanism of gas hydrates at the molecular scale.<sup>27–34</sup> Numerous MD simulations explored the effects of surface properties,<sup>35–38</sup> charge distribution,<sup>39,40</sup> organic matter–clay synergy,<sup>41–43</sup> pore size,<sup>44–46</sup> clay stacking,<sup>47</sup> marine environment,<sup>48,49</sup> and gas nanobubble<sup>50,51</sup> on the formation of gas hydrates in oceanic sediments. In prior MD studies, the positions of clay models are infinitely extended flat nanoplates, which may differ significantly from actual clay particles.<sup>52–55</sup> These models assumed fixed positions and rigid structures for the clay particles, which do not adequately reflect the flexible nature of clay minerals in real sedimentary environments. In fact, natural clays (such as montmorillonite) are pseudo-hexagonal flexible nanoparticles with diameters of ~10–1000 nm.<sup>56</sup> Although several studies had developed molecular models of clay particles,<sup>57–59</sup> no study reported on gas hydrate formation in pseudo-hexagonal flexible clay sediments. In real hydrate-bearing sediments, mixed clays are often found; prior studies focused on the formation of gas hydrates in pure clays. Knowledge of the formation mechanism of gas hydrates in mixed clay sediments is essential for comprehending the formation of hydrate-bearing marine sediments.<sup>60</sup>

In this study, we propose a new molecular model of pseudo-hexagonal montmorillonite nanoparticles and perform large-scale force field-based MD simulations to study the formation of CH<sub>4</sub> and CH<sub>4</sub>/CO<sub>2</sub> hydrates in montmorillonite–illite mixed clay sediments with surface defects. The results indicate that CH<sub>4</sub> and CH<sub>4</sub>/CO<sub>2</sub> hydrates are concentrated inside and outside the clay defects, but these hydrates are challenging to form at the junction

between them. CH<sub>4</sub> and CH<sub>4</sub>/CO<sub>2</sub> mixed hydrates exhibit a preference for forming outside the clay defects rather than inside them. The molecular model of pseudo-hexagonal montmorillonite nanoparticles advances the development of clay particle models. This molecular insight into the formation of pure CH<sub>4</sub> hydrates and CH<sub>4</sub>/CO<sub>2</sub> mixed hydrates in montmorillonite–illite mixed clay sediments expands an understanding of natural gas hydrate accumulation and hydrate-based CO<sub>2</sub> sequestration. This paper is organized as follows: Sec. II provides the technical details and initial model of molecular simulation. More details on the molecular simulation techniques are provided in the [supplementary material](#); Sec. III discusses the performance of the pseudo-hexagonal montmorillonite model and elucidates the formation mechanism of CH<sub>4</sub> and CH<sub>4</sub>/CO<sub>2</sub> hydrates in montmorillonite–illite mixed clay sediments; and Sec. IV presents the conclusions.

## II. SIMULATION MODELS AND METHODS

The initial configuration was composed of pseudo-hexagonal montmorillonite nanoparticles, illite clay, and homogeneous solution, as shown in Fig. 1. Pseudo-hexagonal montmorillonite nanoparticles were generated by cutting montmorillonite nanoplates. The process is as follows: (1) Montmorillonite nanoplates were obtained by expanding the unit cell of montmorillonite;<sup>61</sup> (2) the montmorillonite nanoplates were cut into pseudo-hexagonal montmorillonite nanoparticles; and (3) the cut-edge surfaces of montmorillonite nanoparticles were hydroxylated.<sup>48,55</sup> This modification is necessary, as the edges of clay particles tend to undergo hydroxylation due to interactions with water and other ions in natural systems. To maintain charge neutrality of the edge local structures and the overall nanoparticles, the charge distribution of atoms on the edge surface was adjusted (see Fig. S1). The diameter of the pseudo-hexagonal montmorillonite nanoparticles was about 12 nm, which is the same magnitude as the diameter of montmorillonite particles in real reservoirs.<sup>56</sup> The model closely matches the size and shape of real montmorillonite particles encountered in natural marine sediments. The novel molecular model of pseudo-hexagonal montmorillonite nanoparticles distinguishes itself from previous models. Our model considers flexibility, where the montmorillonite nanoparticle can deform under external forces,

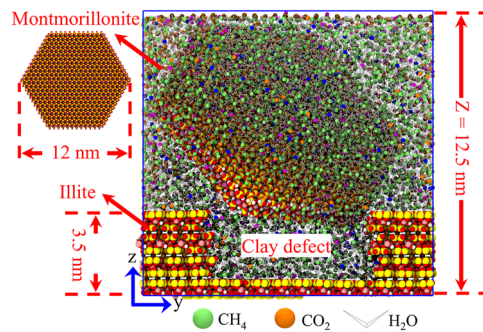


**FIG. 1.** Schematic representation of the initial configuration. Pseudo-hexagonal montmorillonite nanoparticle and illite layers are displayed as yellow (Si atom), pink (Al atom), red (O atom), and white (H atom). Green and orange balls represent the CH<sub>4</sub> and CO<sub>2</sub> molecules, respectively.

as observed under real conditions (Fig. 1). This flexibility allows for more accurate simulations of interactions between clay particles and gas/water molecules. The illite minerals were the most abundant clay mineral in the hydrate-bearing sediments in the Shenhua area of the South China Sea.<sup>8,9</sup> The illite model was an infinitely extended nanoplate and contained surface defects. The clay defect is a common feature of clay minerals and often appears in actual situations.<sup>62</sup> Natural illite particles in hydrate-bearing sediments contain edge defects and surface irregularities, which influence the interactions between the clay minerals and other molecules, such as water and gas molecules. To study the influence of clay defects on hydrate formation, an illite model with surface defects was constructed, and the defect edges were also hydroxylated. The homogeneous solution is composed of 4424 gas molecules, 25 440 water molecules, and 1224 ions (Table S1). The gas mole fraction in water was set to 0.148, which is consistent with the gas–water ratio of the standard SI-type hydrate crystal. In total, two systems containing different gases (pure CH<sub>4</sub> or a mixture of CH<sub>4</sub> and CO<sub>2</sub>) in montmorillonite–illite mixed sediments were tested. We refer to these two systems hereafter as mixed<sub>CH<sub>4</sub></sub> and mixed<sub>CH<sub>4</sub>+CO<sub>2</sub></sub>. The mixed<sub>CH<sub>4</sub></sub> and mixed<sub>CH<sub>4</sub>+CO<sub>2</sub></sub> systems contained ~13 600 and 14 500 atoms, respectively. Initial configuration files for these two systems studied here are shown in Files S1 and S2 of the [supplementary material](#). To test the mechanical properties of pseudo-hexagonal montmorillonite nanoparticles, the nanoparticles were subjected to tension, compression, and shear [Figs. S2(a)–S2(c)]. All mechanical simulations were performed using the pull module of the GROMACS 2022<sup>63</sup> software.

The pseudo-hexagonal montmorillonite nanoparticle, illite nanoplate with surface defects, and ions (Cl<sup>−</sup>, Na<sup>+</sup>, and K<sup>+</sup>) were represented using the ClayFF.<sup>64</sup> The CH<sub>4</sub>, CO<sub>2</sub>, and H<sub>2</sub>O molecules were modeled using the OPLS-UA,<sup>65</sup> TraPPE,<sup>66</sup> and TIP4P-Ice<sup>67</sup> force fields, respectively. Details on the force field parameters are provided in the [supplementary material](#) (Tables S2 and S3). The force field parameters for the pseudo-hexagonal montmorillonite nanoparticles were carefully adjusted to account for the flexibility of the nanoparticle and its edge structures. This was necessary to ensure charge neutrality and accurate interactions between clay surfaces and gas/water molecules. The well depth  $\varepsilon_{O(CO_2)}-O(H_2O)$  between the oxygen in CO<sub>2</sub> and the oxygen in H<sub>2</sub>O was scaled by a factor of 1.08. It has been demonstrated that with such scaling, the solubility of CO<sub>2</sub> in water and the three-phase coexistence temperature of CO<sub>2</sub> hydrate can be accurately predicted.<sup>68</sup> Initially, the initial configurations were energy minimized by using the steepest descent algorithm. A 2-ns pre-equilibration was performed in the isothermal–isobaric (*NPT*) ensemble, with the temperature (260 K)

and pressure (100 bars) controlled by a velocity-rescaling thermostat<sup>69</sup> (time constants of 0.1 ps) and the Berendsen barostat<sup>70</sup> (time constants of 1.0 ps), respectively. The condition of low temperature and high pressure accelerates hydrate formation and reduces the computational cost.<sup>48</sup> Finally, a 3.0 μs production run was carried out at the *NPT* ensemble, with temperature ( $T = 260$  K) and pressure ( $P = 100$  bars) controlled by the Nosé–Hoover thermostat<sup>71</sup> (time constants of 2.0 ps) and Parrinello–Rahman barostat<sup>72</sup> (time constants of 4.0 ps), respectively. The xy-plane of the illite layer, being infinite and rigid, would not compress significantly even under varying pressure conditions (Fig. S3). The pressure coupling was semi-isotropic, allowing independent fluctuations along the normal (z-dimension) and lateral (xy-dimensions) directions. The leap-frog integrator algorithm with a time step of 2.0 fs was used. The particle mesh Ewald (PME) method with a cutoff range of 10 Å was used to determine the long-range Coulombic interactions using a grid spacing of 1.2 Å. The cutoff range of 10 Å was applied to compute the van der Waals forces. Periodic boundary conditions were assigned in all directions. The illite nanoplate with surface defects was fixed with a force of 1000 kJ mol<sup>−1</sup> nm<sup>−2</sup> to prevent illite deformation, which was often used in prior studies.<sup>40,43</sup> The pseudo-hexagonal montmorillonite nanoparticle was flexible in the simulation box. All the simulations above were performed using the GROMACS 2022<sup>63</sup> package. Details of the simulation scheme and calculation principle were provided in the [supplementary material](#).

### III. RESULTS AND DISCUSSIONS

#### A. Mechanical properties of pseudo-hexagonal montmorillonite nanoparticle

To verify the mechanical properties of the pseudo-hexagonal montmorillonite nanoparticle, we subjected it to tensile, compressive, and shear deformations. The stress–strain curves of mechanical deformation are shown in Figs. 2(a)–2(c). The results indicate that the stress–strain curves of tension, compression, and shear of pseudo-hexagonal montmorillonite nanoparticles exhibit linear characteristics (strain from 0 to 0.018). During the tensile deformation process, the tensile stress increases linearly with the increase in tensile strain [Fig. 2(a)]. The elastic modulus of tension ( $E_T$ ) for pseudo-hexagonal montmorillonite nanoparticles is calculated to be ~435 GPa [Fig. 2(a)]. This value falls within the range reported in the literature (range 400–695.8 GPa). The simulation results of Manevitch and Rutledge<sup>73</sup> show that the elastic modulus of tension for montmorillonite nanoplates is 400–420 GPa (strain from 0 to 0.016), while Ghazanfari *et al.*<sup>74</sup> calculated the elastic modulus of tension for montmorillonite nanoplates to be 695.8 GPa

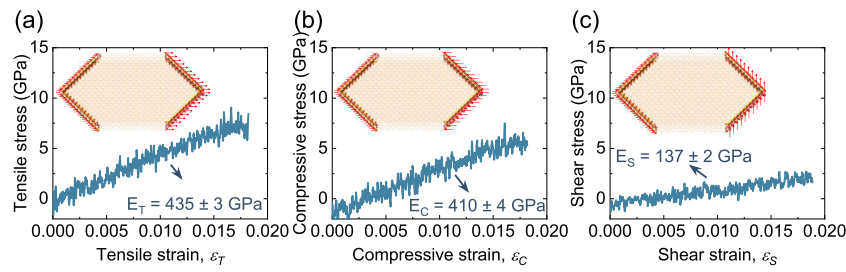


**FIG. 2.** Mechanical (a) tensile, (b) compressive, and (c) shear stress–strain curves of pseudo-hexagonal montmorillonite nanoparticles.

(strain from 0 to 0.009). This shows that the tensile properties of the developed pseudo-hexagonal montmorillonite nanoparticles are similar to those of montmorillonite nanoplates. During the compressive deformation process, the compressive stress increases linearly with the increase in compressive strain [Fig. 2(b)]. The elastic modulus of compression for pseudo-hexagonal montmorillonite nanoparticles is  $\sim 410$  GPa, which is slightly lower than the elastic modulus of tension [Figs. 2(a) and 2(b)]. During the shear deformation process, the shear stress also increases linearly with the increase in shear strain [Fig. 2(c)]. The shear modulus of pseudo-hexagonal montmorillonite nanoparticles is  $\sim 137$  GPa, which is significantly lower than both tensile modulus and compression modulus [Figs. 2(a)–2(c)]. The shear modulus of all-atomic montmorillonite nanoplates reported by Ghazanfari *et al.*<sup>74</sup> is 137 GPa (strain from 0 to 0.04), which is similar to the shear modulus of the pseudo-hexagonal montmorillonite nanoparticles developed here. In summary, the mechanical properties of the pseudo-hexagonal montmorillonite nanoparticles developed in this study are similar to those of previous studies of montmorillonite nanoplates. The tensile, compressive, and shear moduli of pseudo-hexagonal montmorillonite nanoparticles calculated here provide a basis for subsequent related research. However, due to the limitations of the simulation, we focus on the elastic regime and do not explore the ultimate tensile stress and strain values. The limitations in reaching the ultimate tensile stress and strain values are primarily due to the computational constraints of simulation time and spatial scale, rather than the model itself. Beyond this strain range, nonlinear behavior and potential failure will occur. Future studies can extend the simulation to observe the failure point. Moreover, montmorillonite nanoparticles are subject to complex environments in nature or experiments, including flow, heat transfer, vibration, and reaction. Our study focuses on gas hydrate formation under static conditions with controlled temperature and pressure. In future studies, we can consider the effects of complex environments on pseudo-hexagonal montmorillonite nanoparticles, e.g., chemical reactions or heat transfer processes.

## B. CH<sub>4</sub> hydrate formation in montmorillonite–illite mixed clay sediments

The formation of CH<sub>4</sub> hydrates in oceanic sediments is profoundly influenced by the presence of clay defects. The results show

that CH<sub>4</sub> hydrates form quickly inside the clay defects and near pseudo-hexagonal montmorillonite nanoparticles (i.e., outside the clay defects) but are difficult to form at the junction of inside and outside clay defects. During the 3.0  $\mu$ s period of CH<sub>4</sub> hydrate formation, a lot of CH<sub>4</sub> hydrates form inside the clay defects and near pseudo-hexagonal montmorillonite nanoparticles [Figs. 3(a)–3(g) and S4(a)–S4(f)]. CH<sub>4</sub> molecules in montmorillonite–illite mixed clay sediments are widely distributed both inside and outside the clay defects [Figs. 4(a), S5(a), and S5(b)]. Initially, high concentrations of CH<sub>4</sub> in the homogeneous solution lead to the formation of large CH<sub>4</sub> nanobubbles inside and outside the clay defects [Figs. 3(b) and 3(e)]. As the simulation progresses, the formation of CH<sub>4</sub> hydrates consumes carbon sources, causing the CH<sub>4</sub> nanobubbles to diminish in size [Figs. S6(a)–S6(c)]. H<sub>2</sub>O molecules are adsorbed on both the inner and outer surfaces of clay defects, whereas CH<sub>4</sub> molecules do not show significant adsorption peaks on the inner and outer surfaces of clay defects [Figs. 4(a), S5(a), and S5(b)]. This indicates that CH<sub>4</sub> molecules are not easily adsorbed on the inner and outer surfaces of clay defects, while H<sub>2</sub>O molecules can be adsorbed to these surfaces [Figs. S6(a)–S6(c) and S7(a)–S7(c)]. This is mainly due to the presence of adsorbed ions (e.g., Na<sup>+</sup> and K<sup>+</sup>), which reduce the availability of adsorption sites for CH<sub>4</sub> molecules. The ions tend to occupy the clay surfaces, creating a shielding effect that hinders direct interactions between CH<sub>4</sub> and the clay surface [Figs. S8(a)–S8(c)]. CH<sub>4</sub> molecules exhibit an adsorption behavior near the pseudo-hexagonal montmorillonite nanoparticles [Figs. 3(b)–3(d)]. This is due to the absence of significant ion coverage on the outer surfaces of the clay particles, allowing more CH<sub>4</sub> molecules to interact directly with the nanoparticle surface [Figs. 3(b)–3(d)]. These gas molecules will adsorb on the surface of the pseudo-hexagonal montmorillonite nanoparticle [Figs. 3(b)–3(d)]. This adsorption behavior is consistent with observations from previous studies on montmorillonite nanoplate models,<sup>39,40</sup> confirming the validity of our nanoparticle model in simulating real interactions.

The  $F_4$  order parameter<sup>75</sup> for water molecules can accurately identify hydrate formation, with average values of  $-0.04$  and  $0.7$  for liquid water and hydrate, respectively. The time evolution of the value of  $F_4$  along the z-axis is shown in Fig. 4(b). After 0.2  $\mu$ s, the values of  $F_4$  along the z-axis increase rapidly, suggesting that the CH<sub>4</sub> hydrates rapidly nucleate and then grow inside and outside the clay defects [Fig. 4(b)]. At the junction between the inside and

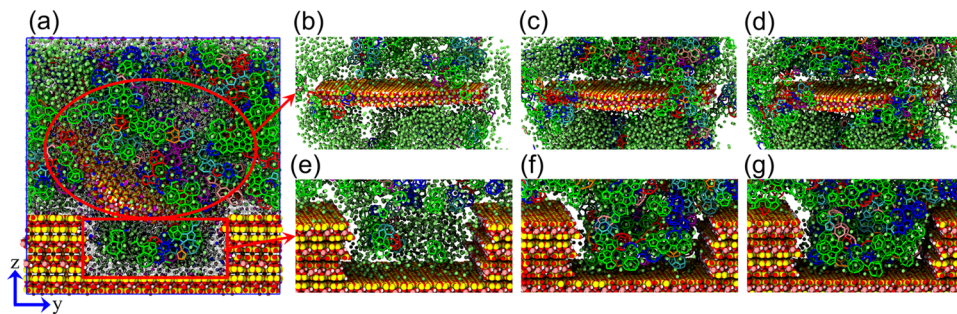


**FIG. 3.** (a) Snapshots of CH<sub>4</sub> hydrates in montmorillonite–illite mixed clay sediments at 3  $\mu$ s. Formation processes of CH<sub>4</sub> hydrates (b)–(d) near the pseudo-hexagonal montmorillonite nanoparticle and (e)–(g) inside the clay defects at 0.2, 1.0, and 3.0  $\mu$ s are shown, respectively. Pseudo-hexagonal montmorillonite nanoparticle and illite layers are displayed as yellow for Si, pink for Al, red for O, and white for H. Green balls represent CH<sub>4</sub> molecules. Hydrate cages are shown as green ( $5^{12}$ ), blue ( $5^{12}6^2$ ), red ( $5^{12}6^3$ ), orange ( $5^{12}6^4$ ), cyan ( $4^{15}106^2$ ), purple ( $4^{15}106^3$ ), and pink sticks ( $4^{15}106^4$ ).

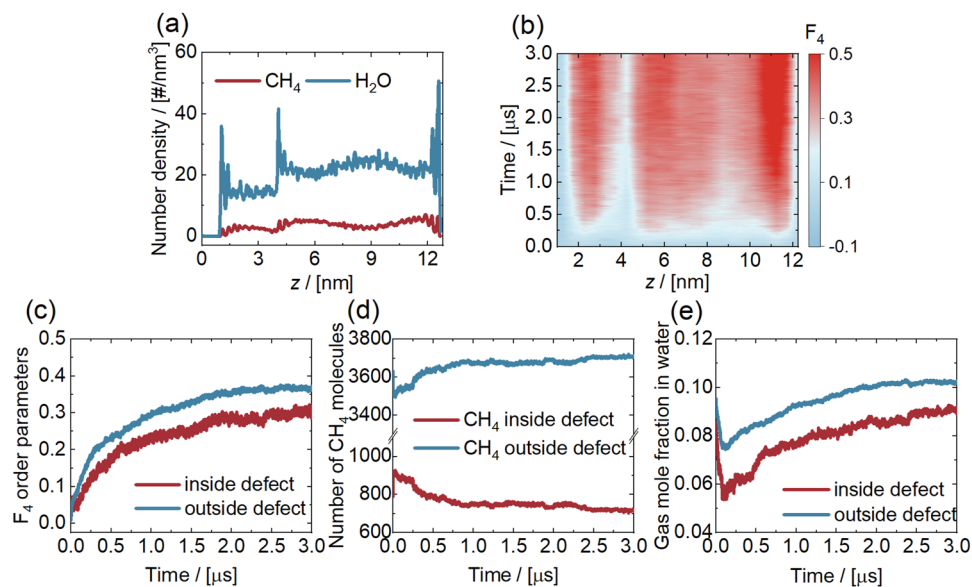


**FIG. 4.** (a) Density distribution curves of H<sub>2</sub>O and CH<sub>4</sub> molecules for 2.95–3.0  $\mu$ s and (b) time evolution of  $F_4$  along the z-axis direction in the mixed<sub>CH4</sub> system. Time evolution of (c) the  $F_4$  order parameters, (d) the number of CH<sub>4</sub> molecules, and (e) gas mole fraction inside and outside the clay defects. The range inside the clay defects is  $\sim$ 0 nm  $<$  z  $<$  3.5 nm, while the range outside the clay defects is  $\sim$ 3.5 nm  $<$  z  $<$  12.5 nm.

outside clay defects ( $z = 3.5\text{--}4.0$  nm), the value of  $F_4$  at the junction remains low [Fig. 4(b)]. This suggests that CH<sub>4</sub> hydrates are primarily concentrated inside and outside the clay defects but are difficult to form at the junction between the inside and outside clay defects [Fig. 4(b)]. This phenomenon may be due to the mass transfer of CH<sub>4</sub>/H<sub>2</sub>O molecules inside and outside the clay defects. This means that in the real hydrate accumulation process, CH<sub>4</sub> hydrates are formed at the junction of inside and outside clay defects after a long time, potentially rendering the CH<sub>4</sub> hydrates at this location less stable. During the subsequent hydrate production process, the CH<sub>4</sub> hydrates at the junction may be more prone to preferential decomposition and mechanical disruption. The formation process of CH<sub>4</sub> hydrates in mixed clay sediments studied here is shown in Video S1 of the [supplementary material](#).

The range inside the clay defects is  $\sim$ 0 nm  $<$  z  $<$  3.5 nm, while the range outside the clay defects is  $\sim$ 3.5 nm  $<$  z  $<$  12.5 nm (see Fig. 1). The time evolution of the  $F_4$  order parameters, the number of CH<sub>4</sub> molecules, and CH<sub>4</sub> mole fraction in water inside and outside the clay defects are shown in Figs. 4(c)–4(e), respectively. CH<sub>4</sub> hydrates exhibit a preference for forming outside the clay defects rather than inside the clay defects. Although the values of  $F_4$  both inside and outside the clay defects increase as a function of time, the values of  $F_4$  outside the clay defects are always higher than the values of  $F_4$  inside the clay defects [Fig. 4(c)]. This shows that CH<sub>4</sub> hydrates prefer to form outside the clay defects. During the 3.0  $\mu$ s period of CH<sub>4</sub> hydrate formation, the number of CH<sub>4</sub> molecules inside the clay defects decreases from  $\sim$ 900 to 700, while the number of CH<sub>4</sub> molecules outside the clay defects increases from about 3500 to 3700 [Fig. 4(d)]. The nucleation and growth of CH<sub>4</sub> hydrates require a sufficient carbon source; thus, the mass transfer of CH<sub>4</sub> molecules inside and outside the clay defects affects CH<sub>4</sub> hydrate formation. The mass transfer of CH<sub>4</sub> molecules is conducive to the formation of CH<sub>4</sub> hydrates outside the clay defects rather than inside them. It is also observed from Fig. 4(a) that CH<sub>4</sub> molecules have an adsorption behavior outside the clay defects. This differential

behavior inside and outside the defects suggests that while clay defects provide nucleation sites, the actual growth of CH<sub>4</sub> hydrates is more likely to occur outside the defects where the physical conditions are more favorable for gas adsorption and subsequent hydrate formation. This mechanism is critical in understanding the accumulation process of natural gas hydrate in mixed clay sediments. During the 0–0.1  $\mu$ s period of CH<sub>4</sub> hydrate formation, CH<sub>4</sub> molecules in the homogeneous solution inside and outside the clay defects quickly form nanobubbles to the water phase [Figs. S6(a)–S6(c)]. Therefore, CH<sub>4</sub> molecules in the water inside and outside the clay defects decrease, while CH<sub>4</sub> molecules in the nanobubbles increase [Figs. S9(a) and S9(b)], which reduces the CH<sub>4</sub> mole fraction in the water inside and outside the clay defects [Fig. 4(e)]. A high mole fraction of guest molecules in the water phase is crucial for promoting hydrate formation.<sup>60</sup> Subsequently (during 0.1–3  $\mu$ s), the CH<sub>4</sub> nanobubbles diminish in size as a function of time [Figs. S6(a)–S6(c)]. More CH<sub>4</sub> molecules migrate from the nanobubbles to the water phase [Figs. S9(a) and S9(b)], increasing the CH<sub>4</sub> concentration dissolved in the water and thereby facilitating the formation of CH<sub>4</sub> hydrate cages [Fig. 4(e)]. The CH<sub>4</sub> hydrate cages in montmorillonite–illite mixed clay sediments are mainly 5<sup>12</sup> small cages, followed by 5<sup>12</sup>6<sup>2</sup> and 4<sup>5</sup>10<sup>6</sup>2 small cages [Figs. S10(a) and S10(b)], consistent with previous research results.<sup>48,60</sup> By the end of CH<sub>4</sub> hydrate formation (at 3  $\mu$ s), about 1200 hydrate cages are formed in montmorillonite–illite mixed clay sediments [Fig. S10(b)].

### C. CH<sub>4</sub>/CO<sub>2</sub> hydrate formation in montmorillonite–illite mixed clay sediments

The formation of CH<sub>4</sub>/CO<sub>2</sub> mixed hydrates in montmorillonite–illite mixed sediments is also influenced by the presence of clay defects. The results show that CH<sub>4</sub>/CO<sub>2</sub> mixed hydrates form quickly both inside and outside the clay defects, but they are challenging to form at the junction between the inside and outside clay defects. The snapshots of CH<sub>4</sub>/CO<sub>2</sub> mixed hydrates in

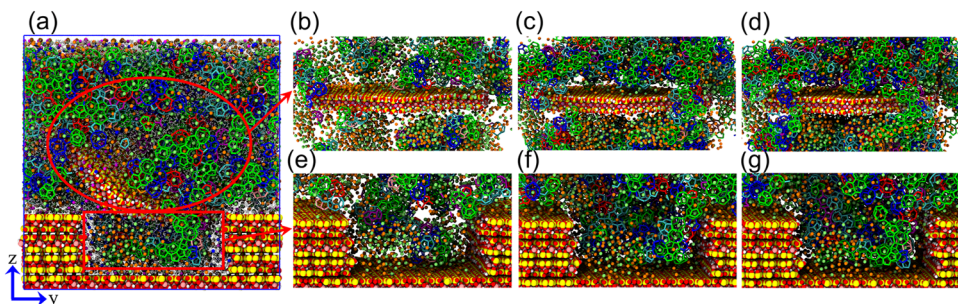


**FIG. 5.** (a) Snapshot of  $\text{CH}_4/\text{CO}_2$  mixed hydrates in montmorillonite–illite clay sediments at 3  $\mu\text{s}$ . Formation processes of  $\text{CH}_4/\text{CO}_2$  mixed hydrates (b)–(d) near the pseudo-hexagonal montmorillonite nanoparticle and (e)–(g) inside the clay defects at 0.2, 1.0, and 3.0  $\mu\text{s}$  are shown. Green balls, orange balls, and silver lines represent the  $\text{CH}_4$ ,  $\text{CO}_2$ , and  $\text{H}_2\text{O}$  molecules, respectively.

montmorillonite–illite clay sediments are shown in Figs. 5(a)–5(g) and S11(a)–S11(f). A large number of  $\text{CH}_4/\text{CO}_2$  mixed hydrate cages are observed in montmorillonite–illite mixed clay sediments [Figs. 5(a)–5(g) and S11(a)–S11(f)].  $\text{CO}_2$  molecules are adsorbed on the inner and outer surfaces of clay defects to form adsorption peaks [Figs. 6(a), S12(a), S12(b), and S13(a)–S13(c)]. The differences in the distribution of  $\text{CH}_4$ ,  $\text{H}_2\text{O}$ , and ions in the mixed <sub>$\text{CH}_4+\text{CO}_2$</sub>  system are small compared to those observed in the mixed <sub>$\text{CH}_4$</sub>  system [Figs. S14(a)–S14(c), S15(a)–S15(c), and S16(a)–S16(c)]. Supersaturated  $\text{CH}_4/\text{CO}_2$  concentrations lead to the formation of  $\text{CH}_4/\text{CO}_2$  mixed nanobubbles both inside and outside the clay defects. As  $\text{CH}_4/\text{CO}_2$  mixed hydrates form, the size of  $\text{CH}_4/\text{CO}_2$  mixed nanobubbles becomes gradually small [Figs. S13(a)–S13(c) and S14(a)–S14(c)]. The value of  $F_4$  inside and outside the clay defects is greater than 0.3, while the value of  $F_4$  at the junction of inside and outside clay defects remains always low. The value of  $F_4$  at the junction of inside and outside clay defects is less than 0.3 [Fig. 6(b)]. This indicates that  $\text{CH}_4/\text{CO}_2$  mixed hydrates are also difficult to form at the junction of inside and outside clay defects. The formation process of  $\text{CH}_4/\text{CO}_2$  mixed hydrates in montmorillonite–illite clay sediments studied here is shown in Video S2 of the supplementary

material. However, the limited deformation observed in the videos is indeed due to periodic boundary conditions and the relatively small system size in the simulation. These factors inherently constrain the extent to which large-scale deformation can be visualized within our setup. Expanding the system size to include larger montmorillonite nanoparticles or additional particles would substantially increase computational demands. A larger system could potentially allow for more pronounced particle deformation and inter-particle interactions. In future studies, we plan to simulate larger clay nanoparticle systems to capture the interactions and potential deformation between particles on a more realistic scale. This approach would allow us to observe deformations that may not be apparent in smaller, periodic systems.

$\text{CH}_4/\text{CO}_2$  mixed hydrates in montmorillonite–illite clay sediments also exhibit formation preferences. At the end of  $\text{CH}_4/\text{CO}_2$  mixed hydrate formation (3  $\mu\text{s}$ ), the value of  $F_4$  outside the clay defects is about 0.4, while the value of  $F_4$  inside the clay defects is about 0.3 [Fig. 6(c)]. The values of  $F_4$  outside the clay defects are significantly higher than the values of  $F_4$  inside the clay defects, indicating that  $\text{CH}_4/\text{CO}_2$  mixed hydrates also prefer to form outside the clay defects [Fig. 6(c)]. During the

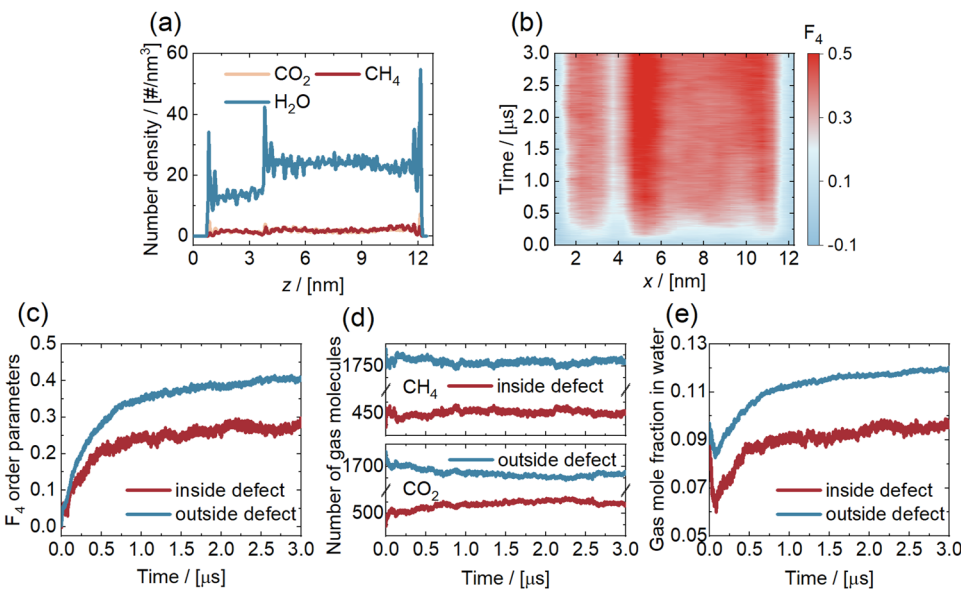


**FIG. 6.** (a) Density distribution curves of  $\text{H}_2\text{O}$ ,  $\text{CH}_4$ , and  $\text{CO}_2$  molecules for 2.95–3.0  $\mu\text{s}$  and (b) time evolution of the  $F_4$  order parameters along the  $z$ -axis direction in the mixed <sub>$\text{CH}_4+\text{CO}_2$</sub>  system. Time evolution of (c) the  $F_4$  order parameters, (d) the number of  $\text{CH}_4/\text{CO}_2$  molecules, and (e) gas mole fraction inside and outside the clay defects.

0–3  $\mu$ s of mixed hydrate formation,  $\text{CH}_4/\text{CO}_2$  mixed nanobubbles are adsorbed on the inner surface of the clay defect [Figs. 5(e)–5(g), S13(a)–S13(c), and S14(a)–S14(c)]. Although the  $\text{CH}_4/\text{CO}_2$  mixed nanobubbles on the inner surface of the clay defect gradually become small as a function of time, they are firmly adsorbed on the inner surface of the clay defect [Figs. 5(e)–5(g), S13(a)–S13(c), and S14(a)–S14(c)]. In contrast, two large  $\text{CH}_4/\text{CO}_2$  mixed nanobubbles outside the clay defects become smaller as a function of time [Figs. 5(b)–5(d), S13(a)–S13(c), and S14(a)–S14(c)]. There is no significant migration of  $\text{CH}_4$  molecules between the inside and outside clay defects, whereas some  $\text{CO}_2$  molecules from the inside clay defect migrate to the outside clay defect [Fig. 6(d)]. This mass transfer of  $\text{CO}_2$  molecules is conducive to the formation of  $\text{CH}_4/\text{CO}_2$  mixed hydrates outside the clay defects. As  $\text{CH}_4/\text{CO}_2$  mixed hydrates form,  $\text{CH}_4/\text{CO}_2$  molecules in the nanobubbles inside and outside the clay defects dissolve in water, increasing the mole fraction of  $\text{CH}_4/\text{CO}_2$  molecules in water inside and outside the clay defects and promoting the formation of  $\text{CH}_4/\text{CO}_2$  mixed hydrates [Figs. 6(e), S17(a), and S17(b)]. The gas mole fraction will experience a rapid decline at the beginning because the excessive gas concentration in the aqueous solution leads to the gradual formation of nanobubbles [Fig. 6(e)]. Subsequently, the gas mole fraction in the aqueous solution gradually increases. The gas mole fraction inside the clay defects increases from 0.06 to 0.098, while the gas mole fraction outside the clay defects increases from 0.085 to 0.12 [Fig. 6(e)]. During the 0–3  $\mu$ s of mixed hydrate formation, the  $\text{CH}_4/\text{CO}_2$  mixed hydrates in montmorillonite–illite clay sediments are mainly composed of  $5^{12}$ ,  $4^{15}10^{6^2}$ , and  $5^{12}6^2$  small cages [Figs. S10(b) and S18]. Compared to the pure  $\text{CH}_4$  hydrate formation in similar sediments, the  $\text{CH}_4/\text{CO}_2$  mixed hydrates contain more  $4^{15}10^{6^2}$  cages [Figs. S10(a), S10(b), and S18].

#### D. Implication for $\text{CH}_4$ recovery and $\text{CO}_2$ sequestration

The insights gained from our MD simulations are applicable to  $\text{CH}_4$  extraction from hydrate sediments and  $\text{CO}_2$  sequestration in marine sediments. The preferential formation of gas hydrates outside the clay defects suggests that strategies for gas extraction and  $\text{CO}_2$  sequestration should focus on the areas where the conditions favor hydrate formation, as there are more gas hydrates outside the clay defects. Understanding the stability of hydrates at the junction between the inside and outside clay defects can provide a reference for methods to maintain reservoir structural integrity in  $\text{CH}_4$  extraction and  $\text{CO}_2$  sequestration. For example, future research can enhance the formation of gas hydrates at junctions or pore throats, which can maintain the integrity of the reservoir structure and reduce environmental hazards. The novel pseudo-hexagonal montmorillonite model developed in this study can be used in large-scale sediment simulations to predict the hydrate behavior in natural environments. This model improves upon previous approaches by accounting for the flexibility and defect structures of clay particles, making it more relevant for simulating real sediment conditions encountered during gas hydrate formation. The migration of gas molecules from inside clay defects to outside clay defects as observed in our simulations is beneficial for recovering the gases trapped inside those defects during the  $\text{CH}_4$  extraction process.

#### IV. CONCLUSIONS

In this study, we propose a novel molecular model of pseudo-hexagonal montmorillonite nanoparticles. The stress–strain curves of tension, compression, and shear of pseudo-hexagonal montmorillonite nanoparticles exhibit linear characteristics, with the tensile, compressive, and shear moduli calculated to be ~435, 410, and 137 GPa, respectively. In addition, we perform microsecond molecular dynamics simulations to study the formation of pure  $\text{CH}_4$  hydrates and  $\text{CH}_4/\text{CO}_2$  mixed hydrates in montmorillonite–illite mixed clay sediments with surface defects. The results show that the formation of pure  $\text{CH}_4$  hydrates and  $\text{CH}_4/\text{CO}_2$  mixed hydrates in montmorillonite–illite mixed clay sediments is profoundly influenced by the presence of clay defects.  $\text{CH}_4$  hydrates and  $\text{CH}_4/\text{CO}_2$  mixed hydrates are challenging to form at the junction between the inside and outside clay defects.  $\text{CH}_4$  hydrates and  $\text{CH}_4/\text{CO}_2$  mixed hydrates exhibit a preference for forming outside the clay defects rather than inside the clay defects. Some  $\text{CH}_4$  and  $\text{CO}_2$  molecules from the inside clay defect migrate to the outside clay defect, thereby promoting the formation of  $\text{CH}_4$  hydrates and  $\text{CH}_4/\text{CO}_2$  mixed hydrates outside the clay defects. This molecular insight into the formation of pure  $\text{CH}_4$  hydrates and  $\text{CH}_4/\text{CO}_2$  mixed hydrates in montmorillonite–illite mixed clay sediments expands an understanding of natural gas hydrate accumulation and hydrate-based  $\text{CO}_2$  sequestration. The development of the pseudo-hexagonal montmorillonite nanoparticle model represents a significant advancement in clay molecular modeling. The tensile, compressive, and shear moduli of pseudo-hexagonal montmorillonite nanoparticles calculated here provide a basis for subsequent related research, e.g., the mechanical properties of hydrate-bearing sediments from the molecular scale. Our group is currently researching the microscopic behavior of systems containing multiple montmorillonite nanoparticles to observe inter-particle interactions and collective behavior in a larger, more complex setup.

#### SUPPLEMENTARY MATERIAL

See the [supplementary material](#) for additional details of the simulation models and methods; parameters and force field for the systems; the final charges of edge atoms for pseudo-hexagonal montmorillonite nanoparticles; calculation of properties; hydrate formation processes; number density distributions of  $\text{H}_2\text{O}$ ,  $\text{CH}_4$ , and  $\text{CO}_2$  ions; number of  $\text{CH}_4/\text{CO}_2$  molecules inside and outside the clay defects; and numbers of seven hydrate cages. VIDEO S1: Formation process of  $\text{CH}_4$  hydrates in the montmorillonite–illite mixed clay sediments for the  $\text{mixed}_{\text{CH}_4}$  system. VIDEO S2: Formation process of  $\text{CH}_4/\text{CO}_2$  mixed hydrates in the montmorillonite–illite mixed clay sediments for the  $\text{mixed}_{\text{CH}_4+\text{CO}_2}$  system. FILE S1: Initial configuration for the  $\text{mixed}_{\text{CH}_4}$  system. FILE S2: Initial configuration for the  $\text{mixed}_{\text{CH}_4+\text{CO}_2}$  system.

#### ACKNOWLEDGMENTS

This work was supported by the National Science Foundation for Distinguished Young Scholars (Grant No. 42225207), Natural Science Foundation of Hubei Province (Grant No. 2021CFA024), and China Scholarship Council (Grant No. CSC202306410133).

The authors acknowledge the use of computational resources of DelftBlue supercomputer, provided by the Delft High Performance Computing Centre (<https://www.tudelft.nl/dhpc>).

## AUTHOR DECLARATIONS

### Conflict of Interest

The authors have no conflicts to disclose.

### Author Contributions

**Fengyi Mi:** Data curation (equal); Formal analysis (equal); Investigation (equal); Methodology (equal); Validation (equal); Visualization (equal); Writing – original draft (equal). **Jiangtao Pang:** Conceptualization (equal); Formal analysis (equal); Writing – review & editing (equal). **Wei Li:** Conceptualization (equal); Formal analysis (equal); Writing – review & editing (equal). **Othonas A. Moulos:** Funding acquisition (equal); Project administration (equal); Supervision (equal); Writing – review & editing (equal). **Fulong Ning:** Conceptualization (equal); Funding acquisition (equal); Project administration (equal); Resources (equal); Supervision (equal); Writing – review & editing (equal). **Thijs J. H. Vlugt:** Conceptualization (equal); Funding acquisition (equal); Project administration (equal); Resources (equal); Supervision (equal); Writing – review & editing (equal).

### DATA AVAILABILITY

The data that support the findings of this study are available within the article and its [supplementary material](#).

### REFERENCES

- <sup>1</sup>C. Zou, Q. Zhao, G. Zhang, and B. Xiong, “Energy revolution: From a fossil energy era to a new energy era,” *Nat. Gas Ind. B* **3**, 1 (2016).
- <sup>2</sup>*Clathrate Hydrates of Natural Gases*, 3rd ed., edited by K. C. Sloan (CRC Press, Boca Raton, FL, 2008), p. 752.
- <sup>3</sup>J. Grabowska, S. Blazquez, E. Sanz, E. G. Noya, I. M. Zeron, J. Algaba, J. M. Miguez, F. J. Blas, and C. Vega, “Homogeneous nucleation rate of methane hydrate formation under experimental conditions from seeding simulations,” *J. Chem. Phys.* **158**, 114505 (2023).
- <sup>4</sup>A. Arjun and P. G. Bolhuis, “Homogeneous nucleation of crystalline methane hydrate in molecular dynamics transition paths sampled under realistic conditions,” *J. Chem. Phys.* **158**, 044504 (2023).
- <sup>5</sup>F. Mi, Z. He, and F. Ning, “Molecular insight on CO<sub>2</sub>/C<sub>3</sub>H<sub>8</sub> mixed hydrate formation from the brine for sustainable hydrate-based desalination,” *Sep. Purif. Technol.* **353**, 128244 (2025).
- <sup>6</sup>C. Chen, Y. Zhang, X. S. Li, J. Y. He, F. Gao, and Z. Y. Chen, “Investigations into methane hydrate formation, accumulation, and distribution in sediments with different contents of illite clay,” *Appl. Energy* **359**, 122661 (2024).
- <sup>7</sup>R. Boswell and T. S. Collett, “Current perspectives on gas hydrate resources,” *Energy Environ. Sci.* **4**, 1206 (2011).
- <sup>8</sup>J. F. Li, J. L. Ye, X. W. Qin, H. J. Qiu, N. Y. Wu, H. L. Lu, W. W. Xie, J. A. Lu, F. Peng, Z. Q. Xu *et al.*, “The first offshore natural gas hydrate production test in South China Sea,” *China Geol.* **1**, 5 (2018).
- <sup>9</sup>J.-l. Ye, X.-w. Qin, W.-w. Xie, H.-l. Lu, B.-j. Ma, H.-j. Qiu, J.-q. Liang, J.-a. Lu, Z.-g. Kuang, C. Lu *et al.*, “The second natural gas hydrate production test in the South China Sea,” *China Geol.* **3**, 197 (2020).
- <sup>10</sup>A. N. Rehman, C. B. Bavoh, R. Pendyala, and B. Lal, “Research advances, maturation, and challenges of hydrate-based CO<sub>2</sub> sequestration in porous media,” *ACS Sustainable Chem. Eng.* **9**, 15075 (2021).
- <sup>11</sup>F. Mi, W. Li, J. Pang, O. A. Moulos, F. Ning, and T. J. H. Vlugt, “Molecular insights into the microscopic behavior of CO<sub>2</sub> hydrates in oceanic sediments: Implications for carbon sequestration,” *J. Phys. Chem. C* **128**, 18588 (2024).
- <sup>12</sup>H. Tanaka, M. Matsumoto, and T. Yagasaki, “Efficiency and energy balance for substitution of CH<sub>4</sub> in clathrate hydrates with CO<sub>2</sub> under multiple-phase coexisting conditions,” *J. Chem. Phys.* **159**, 194504 (2023).
- <sup>13</sup>S. Yu, X. W. Zhang, J. W. Liu, Y. H. Lee, and X. S. Li, “Natural gas hydrate resources and hydrate technologies: A review and analysis of the associated energy and global warming challenges,” *Energy Environ. Sci.* **14**, 5611 (2021).
- <sup>14</sup>F. Ning, Y. Yu, S. Kjelstrup, T. J. H. Vlugt, and K. Glavatskiy, “Mechanical properties of clathrate hydrates: Status and perspectives,” *Energy Environ. Sci.* **5**, 6779 (2012).
- <sup>15</sup>Z. Zhang, L. Liu, W. Lu, C. Liu, F. Ning, and S. Dai, “Permeability of hydrate-bearing fine-grained sediments: Research status, challenges and perspectives,” *Earth-Sci. Rev.* **244**, 104517 (2023).
- <sup>16</sup>X. Kou, H. Zhang, X.-S. Li, Z.-Y. Chen, and Y. Wang, “Methane hydrate phase transition in marine clayey sediments: Enhanced structure change and solid migration,” *Appl. Energy* **368**, 123485 (2024).
- <sup>17</sup>H. Tang, Y. Li, W. Bao, P. Wang, X. Wang, Q. Su, Y. Zhao, J. Zhu, and S. Han, “Methane hydrate formation in clay mineral suspensions containing glycine: Experimental study and molecular dynamics simulation,” *J. Mol. Liq.* **390**, 123124 (2023).
- <sup>18</sup>S. B. Cha, H. Ouari, T. R. Wildeman, and E. D. Sloan, “A third-surface effect on hydrate formation,” *J. Phys. Chem.* **92**, 6492 (2002).
- <sup>19</sup>S. Guggenheim and A. F. Koster van Groos, “New gas-hydrate phase: Synthesis and stability of clay–methane hydrate intercalate,” *Geology* **31**, 653 (2003).
- <sup>20</sup>S.-H. Park and G. Sposito, “Do montmorillonite surfaces promote methane hydrate formation? Monte Carlo and molecular dynamics simulations,” *J. Phys. Chem. B* **107**, 2281 (2003).
- <sup>21</sup>Y. J. Seo, J. Seol, S. H. Yeon, D. Y. Koh, M. Cha, S. P. Kang, Y. T. Seo, J. J. Bahk, J. Lee, and H. Lee, “Structural, mineralogical, and rheological properties of methane hydrates in smectite clays,” *J. Chem. Eng. Data* **54**, 1284 (2009).
- <sup>22</sup>Y. Xie, L. Cheng, J. Feng, T. Zheng, Y. Zhu, X. Zeng, C. Sun, and G. Chen, “Kinetics behaviors of CH<sub>4</sub> hydrate formation in porous sediments: Non-unidirectional influence of sediment particle size on hydrate formation,” *Energy* **289**, 130021 (2024).
- <sup>23</sup>Z. Liu, J. Kim, L. Lei, F. Ning, and S. Dai, “Tetrahydrofuran hydrate in clayey sediments—Laboratory formation, morphology, and wave characterization,” *J. Geophys. Res.: Solid Earth* **124**, 3307, <https://doi.org/10.1029/2018jb017156> (2019).
- <sup>24</sup>D. Jin and B. Coasne, “Reduced phase stability and faster formation/dissociation kinetics in confined methane hydrate,” *Proc. Natl. Acad. Sci. U. S. A.* **118**, e2024025118 (2021).
- <sup>25</sup>J. Ren, X. Liu, M. Niu, and Z. Yin, “Effect of sodium montmorillonite clay on the kinetics of CH<sub>4</sub> hydrate—implication for energy recovery,” *Chem. Eng. J.* **437**, 135368 (2022).
- <sup>26</sup>J. Ren, S. Zeng, D. Chen, M. Yang, P. Linga, and Z. Yin, “Roles of montmorillonite clay on the kinetics and morphology of CO<sub>2</sub> hydrate in hydrate-based CO<sub>2</sub> sequestration,” *Appl. Energy* **340**, 120997 (2023).
- <sup>27</sup>X. Cai, J. Worley, A. Phan, M. Salvaglio, C. Koh, and A. Striolo, “Understanding the effect of moderate concentration SDS on CO<sub>2</sub> hydrates growth in the presence of THF,” *J. Colloid Interface Sci.* **658**, 1 (2024).
- <sup>28</sup>S. Blazquez, J. Algaba, J. M. Miguez, C. Vega, F. J. Blas, and M. M. Conde, “Three-phase equilibria of hydrates from computer simulation. I. Finite-size effects in the methane hydrate,” *J. Chem. Phys.* **160**, 164721 (2024).
- <sup>29</sup>Á. M. Fernández-Fernández, Á. Bárcena, M. M. Conde, G. Pérez-Sánchez, M. Pérez-Rodríguez, and M. M. Piñeiro, “Modeling oceanic sedimentary methane hydrate growth through molecular dynamics simulation,” *J. Chem. Phys.* **160**, 144107 (2024).
- <sup>30</sup>C. L. Bassani, M. Engel, and A. K. Sum, “Mesomorphology of clathrate hydrates from molecular ordering,” *J. Chem. Phys.* **160**, 190901 (2024).
- <sup>31</sup>L. Wang and P. G. Kusalik, “Understanding why constant energy or constant temperature may affect nucleation behavior in MD simulations: A study of gas hydrate nucleation,” *J. Chem. Phys.* **159**, 184501 (2023).

- <sup>32</sup>M. J. Torrejon, C. Romero-Guzman, M. M. Pineiro, F. J. Blas, and J. Algaba, "Simulation of the THF hydrate-water interfacial free energy from computer simulation," *J. Chem. Phys.* **161**, 064701 (2024).
- <sup>33</sup>J. Algaba, M. J. Torrejon, and F. J. Blas, "Dissociation line and driving force for nucleation of the nitrogen hydrate from computer simulation," *J. Chem. Phys.* **159**, 224707 (2023).
- <sup>34</sup>J. Algaba, S. Blazquez, J. M. Miguez, M. M. Conde, and F. J. Blas, "Three-phase equilibria of hydrates from computer simulation. III. Effect of dispersive interactions in the methane and carbon dioxide hydrates," *J. Chem. Phys.* **160**, 164723 (2024).
- <sup>35</sup>Y. Li, M. Chen, H. Tang, S. Han, H. Song, P. Wang, Y. Zhao, and J. Zhu, "Insights into carbon dioxide hydrate nucleation on the external basal surface of clay minerals from molecular dynamics simulations," *ACS Sustainable Chem. Eng.* **10**, 6358 (2022).
- <sup>36</sup>Y. Wu, Y. He, T. Tang, and M. Zhai, "Molecular dynamic simulations of methane hydrate formation between solid surfaces: Implications for methane storage," *Energy* **262**, 125511 (2023).
- <sup>37</sup>R. Wang, B. Liao, J. Wang, J. Sun, Y. Wang, J. Wang, Q. Wang, Y. Qu, and R. Cheng, "Microscopic molecular insights into methane hydrate growth on the surfaces of clay minerals: Experiments and molecular dynamics simulations," *Chem. Eng. J.* **451**, 138757 (2023).
- <sup>38</sup>Z. Zhang, P. G. Kusalik, C. Liu, and N. Wu, "Methane hydrate formation in slit-shaped pores: Impacts of surface hydrophilicity," *Energy* **285**, 129414 (2023).
- <sup>39</sup>Y. Li, M. Chen, C. Liu, H. Song, P. Yuan, B. Zhang, D. Liu, and P. Du, "Effects of layer-charge distribution of 2:1 clay minerals on methane hydrate formation: A molecular dynamics simulation study," *Langmuir* **36**, 3323 (2020).
- <sup>40</sup>F. Mi, Z. He, G. Jiang, and F. Ning, "What roles do interlayer cations ( $K^+$ ) and salt ions ( $Na^+$  and  $Cl^-$ ) play in methane hydrate formation in illite nanopore?", *Appl. Clay Sci.* **256**, 107428 (2024).
- <sup>41</sup>H. Ji, D. Chen, C. Zhao, and G. Wu, "Molecular dynamics simulation of methane hydrate formation and dissociation in the clay pores with fatty acids," *J. Phys. Chem. C* **122**, 1318 (2018).
- <sup>42</sup>M. Fengyi, H. Zhongjin, J. Guosheng, and N. Fulong, "Molecular insights into the effects of lignin on methane hydrate formation in clay nanopores," *Energy* **276**, 127496 (2023).
- <sup>43</sup>F. Mi, Z. He, G. Jiang, and F. Ning, "Effect of glucose on  $CH_4$  hydrate formation in clay nanopores and bulk solution: Insights from microsecond molecular dynamics simulations," *ACS Sustainable Chem. Eng.* **12**, 4644 (2024).
- <sup>44</sup>F. Mi, Z. He, B. Fang, F. Ning, and G. Jiang, "Molecular insights into the effects of surface property and pore size of non-swelling clay on methane hydrate formation," *Fuel* **311**, 122607 (2022).
- <sup>45</sup>K. F. Yan, X. S. Li, Z. Y. Chen, Z. M. Xia, C. G. Xu, and Z. Zhang, "Molecular dynamics simulation of the crystal nucleation and growth behavior of methane hydrate in the presence of the surface and nanopores of porous sediment," *Langmuir* **32**, 7975 (2016).
- <sup>46</sup>S. Alavi, I. L. Moudrakovski, C. I. Ratcliffe, and J. A. Ripmeester, "Unusual species of methane hydrate detected in nanoporous media using solid state  $^{13}C$  NMR," *J. Chem. Phys.* **160**, 214709 (2024).
- <sup>47</sup>J. Pang, X. Gao, F. Mi, Z. Zhu, W. Li, X. Cao, Y. Liang, and F. Ning, "New insight into methane hydrate formation at clay-geofluid interface in natural kaolinite-stacking sediments," *Appl. Clay Sci.* **255**, 107400 (2024).
- <sup>48</sup>F. Mi, Z. He, G. Jiang, and F. Ning, "Effects of marine environments on methane hydrate formation in clay nanopores: A molecular dynamics study," *Sci. Total Environ.* **852**, 158454 (2022).
- <sup>49</sup>S. J. Cox, D. J. F. Taylor, T. G. A. Youngs, A. K. Soper, T. S. Totton, R. G. Chapman, M. Arjmandi, M. G. Hodges, N. T. Skipper, and A. Michaelides, "Formation of methane hydrate in the presence of natural and synthetic nanoparticles," *J. Am. Chem. Soc.* **140**, 3277 (2018).
- <sup>50</sup>Z. Li, Y. Deng, S. Rao, and H. Lu, "Methane gas bubbles affecting the formation and distribution of hydrates in kaolinite slit pores: A molecular dynamics study," *Energy Fuels* **37**, 5102 (2023).
- <sup>51</sup>K. Li, B. Chen, M. Yang, Y. Song, and A. K. Sum, "Methane hydrate phase equilibrium considering dissolved methane concentrations and interfacial geometries from molecular simulations," *J. Chem. Phys.* **159**, 244505 (2023).
- <sup>52</sup>J. Chen, J. Xu, Z. Zhang, C. Liu, G. Hu, T. Ding, Y. Hao, and X. Wang, "Insight on the stability of methane hydrate in montmorillonite slits by molecular dynamics simulations," *Appl. Surf. Sci.* **654**, 159413 (2024).
- <sup>53</sup>B. Fang, T. Lü, W. Li, O. A. Moulton, T. J. H. Vlugt, and F. Ning, "Microscopic insights into poly- and mono-crystalline methane hydrate dissociation in Na-montmorillonite pores at static and dynamic fluid conditions," *Energy* **288**, 129755 (2024).
- <sup>54</sup>B. Liao, J. Wang, X. Han, R. Wang, K. Lv, Y. Bai, H. Jiang, Z. Shao, Y. Wang, and J. Sun, "Microscopic molecular insights into clathrate methane hydrates dissociation in a flowing system," *Chem. Eng. J.* **430**, 133098 (2022).
- <sup>55</sup>F. Mi, Z. He, L. Cheng, G. Jiang, and F. Ning, "Molecular dynamics simulation on methane hydrate formation in clay nanopores of edge surfaces," *Appl. Clay Sci.* **243**, 107069 (2023).
- <sup>56</sup>A. Cadene, S. Durand-Vidal, P. Turq, and J. Brendle, "Study of individual Na-montmorillonite particles size, morphology, and apparent charge," *J. Colloid Interface Sci.* **285**, 719 (2005).
- <sup>57</sup>T. R. Underwood and I. C. Bourg, "Large-scale molecular dynamics simulation of the dehydration of a suspension of smectite clay nanoparticles," *J. Phys. Chem. C* **124**, 3702 (2020).
- <sup>58</sup>X. Zheng, T. R. Underwood, and I. C. Bourg, "Molecular dynamics simulation of thermal, hydraulic, and mechanical properties of bentonite clay at 298 to 373 K," *Appl. Clay Sci.* **240**, 106964 (2023).
- <sup>59</sup>Y. Zhang, J. Oestreicher, W. J. Binns, S. Briggs, C. S. Kim, and L. K. Beland, "A coarse-grained interaction model for sodium dominant montmorillonite," *Langmuir* **38**, 13226 (2022).
- <sup>60</sup>F. Mi, Z. He, Y. Zhao, G. Jiang, and F. Ning, "Effects of surface property of mixed clays on methane hydrate formation in nanopores: A molecular dynamics study," *J. Colloid Interface Sci.* **627**, 681 (2022).
- <sup>61</sup>R. T. Downs and M. Hall-Wallace, "The American Mineralogist crystal structure database," *Am. Mineral.* **88**, 247 (2003).
- <sup>62</sup>A. Meunier, "Why are clay minerals small?", *Clay Miner.* **41**, 551 (2006).
- <sup>63</sup>M. J. Abraham, T. Murtola, R. Schulz, S. Páll, J. C. Smith, B. Hess, and E. Lindahl, "GROMACS: High performance molecular simulations through multi-level parallelism from laptops to supercomputers," *SoftwareX* **1–2**, 19 (2015).
- <sup>64</sup>R. T. Cygan, J. J. Liang, and A. G. Kalinichev, "Molecular models of hydroxide, oxyhydroxide, and clay phases and the development of a general force field," *J. Phys. Chem. B* **108**, 1255 (2004).
- <sup>65</sup>W. L. Jorgensen, J. D. Madura, and C. J. Swenson, "Optimized intermolecular potential functions for liquid hydrocarbons," *J. Am. Chem. Soc.* **106**, 6638 (1984).
- <sup>66</sup>J. J. Potoff and J. I. Siepmann, "Vapor–liquid equilibria of mixtures containing alkanes, carbon dioxide, and nitrogen," *AIChE J.* **47**, 1676 (2001).
- <sup>67</sup>J. L. Abascal, E. Sanz, R. Garcia Fernandez, and C. Vega, "A potential model for the study of ices and amorphous water: TIP4P/Ice," *J. Chem. Phys.* **122**, 234511 (2005).
- <sup>68</sup>J. Costandy, V. K. Michalis, I. N. Tsimpanogiannis, A. K. Stubos, and I. G. Economou, "The role of intermolecular interactions in the prediction of the phase equilibria of carbon dioxide hydrates," *J. Chem. Phys.* **143**, 094506 (2015).
- <sup>69</sup>G. Bussi, D. Donadio, and M. Parrinello, "Canonical sampling through velocity rescaling," *J. Chem. Phys.* **126**, 014101 (2007).
- <sup>70</sup>H. J. C. Berendsen, J. P. M. Postma, W. F. Vangunsteren, A. Dinola, and J. R. Haak, "Molecular dynamics with coupling to an external bath," *J. Chem. Phys.* **81**, 3684 (1984).
- <sup>71</sup>S. Nosé, "A molecular dynamics method for simulations in the canonical ensemble," *Mol. Phys.* **52**, 255 (1984).
- <sup>72</sup>M. Parrinello and A. Rahman, "Crystal structure and pair potentials: A molecular-dynamics study," *Phys. Rev. Lett.* **45**, 1196 (1980).
- <sup>73</sup>O. L. Manevitch and G. C. Rutledge, "Elastic properties of a single lamella of montmorillonite by molecular dynamics simulation," *J. Phys. Chem. B* **108**, 1428 (2004).
- <sup>74</sup>S. Ghazanfari, H. M. N. Faisal, K. S. Katti, D. R. Katti, and W. Xia, "A coarse-grained model for the mechanical behavior of Na-montmorillonite clay," *Langmuir* **38**, 4859 (2022).
- <sup>75</sup>L. A. Báez and P. Clancy, "Computer simulation of the crystal growth and dissolution of natural gas hydrates," *Ann. N. Y. Acad. Sci.* **715**, 177 (1994).